



Search for the rare decays $B_s^0 \rightarrow e^+e^-$ and $B^0 \rightarrow e^+e^-$

LHCb collaboration[†]

Abstract

A search for the decays $B_s^0 \rightarrow e^+e^-$ and $B^0 \rightarrow e^+e^-$ is performed using data collected with the LHCb experiment in proton-proton collisions at center-of-mass energies of 7, 8 and 13 TeV, corresponding to integrated luminosities of 1, 2 and 2 fb^{-1} , respectively. No signal is observed. Assuming no contribution from $B^0 \rightarrow e^+e^-$ decays, an upper limit on the branching fraction $\mathcal{B}(B_s^0 \rightarrow e^+e^-) < 9.4 (11.2) \times 10^{-9}$ is obtained at 90 (95) % confidence level. If no $B_s^0 \rightarrow e^+e^-$ contribution is assumed, a limit of $\mathcal{B}(B^0 \rightarrow e^+e^-) < 2.5 (3.0) \times 10^{-9}$ is determined at 90 (95) % confidence level. These upper limits are more than one order of magnitude lower than the previous values.

Published in Phys. Rev. Lett. 124 (2020) 211802

© 2020 CERN for the benefit of the LHCb collaboration. CC BY 4.0 licence.

[†]Authors are listed at the end of this Letter.

Searches for rare particle decays provide ideal probes for contributions from physics processes beyond the Standard Model (SM). Recent measurements of decays involving $b \rightarrow s \ell^+ \ell^-$ transitions (the inclusion of charge-conjugated processes is implied throughout this Letter) hint at deviations from SM predictions in lepton-flavor universality tests [1–6] and thus motivate measurements of decay rates into final states involving leptons. Following the observation of the decay $B_s^0 \rightarrow \mu^+ \mu^-$ [7,8], the search for $B_s^0 \rightarrow e^+ e^-$ and $B^0 \rightarrow e^+ e^-$ decays provides an independent test of lepton-flavor universality. According to SM predictions (calculated from Ref. [9], neglecting QED corrections that are expected to be at the percent level), $B_{(s)}^0 \rightarrow e^+ e^-$ decays have branching fractions of $\mathcal{B}(B_s^0 \rightarrow e^+ e^-) = (8.60 \pm 0.36) \times 10^{-14}$ and $\mathcal{B}(B^0 \rightarrow e^+ e^-) = (2.41 \pm 0.13) \times 10^{-15}$. With contributions beyond the SM, these branching fractions could be significantly larger, reaching values of $\mathcal{O}(10^{-8})$ for $\mathcal{B}(B_s^0 \rightarrow e^+ e^-)$ and $\mathcal{O}(10^{-10})$ for $\mathcal{B}(B^0 \rightarrow e^+ e^-)$ [10]. These values are close to the current experimental bounds of $\mathcal{B}(B_s^0 \rightarrow e^+ e^-) < 2.8 \times 10^{-7}$ and $\mathcal{B}(B^0 \rightarrow e^+ e^-) < 8.3 \times 10^{-8}$ at 90% confidence level (CL) [11], set by the CDF collaboration.

In this Letter a search for $B_s^0 \rightarrow e^+ e^-$ and $B^0 \rightarrow e^+ e^-$ decays is presented using data collected with the LHCb experiment in proton-proton collisions at center-of-mass energies of 7 TeV in 2011, 8 TeV in 2012 and 13 TeV in 2015 and 2016, corresponding to integrated luminosities of 1, 2 and 2 fb^{-1} , respectively. The signal yields are determined from a fit to the data and normalized to those of the $B^+ \rightarrow J/\psi K^+$ decay, where the J/ψ meson decays to $e^+ e^-$, which has a precisely measured branching fraction [12] and a similar dielectron signature in the detector.

The LHCb detector [13, 14] is a single-arm forward spectrometer covering the pseudorapidity range $2 < \eta < 5$, designed for the study of particles containing b or c quarks. The detector includes a high-precision tracking system consisting of a silicon-strip vertex detector surrounding the pp interaction region, a large-area silicon-strip detector located upstream of a dipole magnet with a bending power of about 4 Tm, and three stations of silicon-strip detectors and straw drift tubes placed downstream of the magnet. Different types of charged hadrons are distinguished using information from two ring-imaging Cherenkov detectors. Photons, electrons and hadrons are identified by a calorimeter system consisting of scintillating-pad and preshower detectors, an electromagnetic and a hadronic calorimeter. Muons are identified by a system composed of alternating layers of iron and multiwire proportional chambers.

The online event selection is performed by a trigger [15], which consists of a hardware stage, based on information from the calorimeter and muon systems, followed by a software stage, which applies a full event reconstruction. At the hardware trigger stage, events are required to have a high-energy deposit in the calorimeters associated with a signal electron candidate, or a muon candidate with high transverse momentum p_T , or a photon, electron or hadron candidate with high transverse energy from the decays of other particles from the pp collision. The software trigger requires a two-track secondary vertex with a significant displacement from any primary pp interaction vertex (PV). At least one charged particle must have high p_T and be inconsistent with originating from a PV. A multivariate algorithm [16, 17] is used in the trigger for the identification of secondary vertices consistent with the decay of a b hadron. Simulated samples are used to optimize the candidate selection, estimate selection efficiencies and describe the expected invariant-mass shapes of the signal candidates and background decays. In the simulation, pp collisions are generated using PYTHIA [18] with a specific LHCb configuration [19]. Decays of unstable

particles are described by EVTGEN [20], in which final-state radiation is generated using PHOTOS [21]. The interaction of the generated particles with the detector, and its response, are implemented using the GEANT4 toolkit [22] as described in Ref. [23]. The simulation is corrected for data-simulation differences in B -meson production kinematics, detector occupancy and isolation criteria [24] using $B^+ \rightarrow J/\psi K^+$ and $B_s^0 \rightarrow J/\psi \phi$ decays, with $J/\psi \rightarrow e^+e^-$ and $\phi \rightarrow K^+K^-$. Particle identification variables are calibrated using data from $B^+ \rightarrow J/\psi K^+$ and $D^0 \rightarrow K^-\pi^+$ decays [25]. The calibration data are binned in momentum and pseudorapidity of the particle as well as detector occupancy to account for possible differences in kinematics between the investigated decay and the calibration data.

The $B_{(s)}^0 \rightarrow e^+e^-$ candidates are selected in events passing the trigger requirements by combining two tracks that are inconsistent with originating from any PV in the event and which form a good-quality secondary vertex. The tracks are also required to have a momentum larger than 3 GeV/ c and p_T greater than 500 MeV/ c , and must be identified as electrons using information from the Cherenkov detectors and calorimeters. The dielectron candidate's momentum must be aligned with the vector pointing from a PV (the associated PV) to the two-track vertex and have a considerable transverse component. The candidate must also have an invariant mass in the range [4166, 6566] MeV/ c^2 .

The measured electron momenta are corrected for losses due to bremsstrahlung radiation by adding the momentum of photons consistent with being emitted upstream of the magnet [26]. Candidates in data and simulation are separated into three categories with either zero, one, or both electrons having a bremsstrahlung correction applied. To avoid experimenters' bias, the narrowest dielectron invariant-mass region containing 90 % of simulated $B_s^0 \rightarrow e^+e^-$ decays, corresponding to a range of [4689, 5588] MeV/ c^2 , was removed from the data set until the analysis procedure was finalized.

Candidates for the normalization mode, $B^+ \rightarrow J/\psi K^+$, are constructed similarly, but require an additional track consistent with being a kaon and originating from the same vertex as the dielectron candidate. The dielectron candidate must have an invariant mass in the range [2450, 3176] MeV/ c^2 , consistent with arising from a J/ψ meson decay. In addition, the reconstructed B^+ candidate mass, when the dielectron candidate is constrained to the known J/ψ mass [12], must be above 5175 MeV/ c^2 , suppressing partially reconstructed decays.

A boosted decision tree (BDT) algorithm [27–29] is used to separate $B_{(s)}^0 \rightarrow e^+e^-$ signal from random combinations of two electrons (combinatorial background). The BDT is trained separately for data taking periods 2011–2012 (Run 1) and 2015–2016 (Run 2) on simulated $B_s^0 \rightarrow e^+e^-$ decays as signal proxy and dielectron candidates from data with a mass above 5588 MeV/ c^2 as background proxy. The split between the data taking periods is done to account for changes in the center-of-mass energies and trigger strategies, which significantly impact the data distributions and improve the BDT and the particle identification algorithms in Run 2. It is checked that the data behave consistently across the data-taking periods. The BDT input variables comprise of the following: kinematic information on the electron tracks and B candidate, information on the displacement of the electrons and B candidate from the associated PV, and isolation variables that quantify the compatibility of other tracks in the event with originating from the same decay as the B candidate [24, 30]. Candidates with a BDT response compatible with that of the background are discarded, with the threshold chosen by maximizing the figure of merit $\epsilon_{\text{signal}}/(\sqrt{N_{\text{background}}} + 3/2)$ [31], where ϵ_{signal} is the signal efficiency and

the expected background yield in the signal region is $N_{\text{background}}$.

The final selected data set is separated by data-taking period and by category of bremsstrahlung correction. The branching fraction $\mathcal{B}(B_{(s)}^0 \rightarrow e^+e^-)$ is measured relative to that of the normalization channel via

$$\mathcal{B}(B_{(s)}^0 \rightarrow e^+e^-) = N(B_{(s)}^0 \rightarrow e^+e^-) \times \alpha \times \mathcal{B}(B^+ \rightarrow J/\psi K^+) \times \left(\frac{f_{d(s)}}{f_u}\right)^{-1}, \quad (1)$$

where

$$\alpha \equiv \frac{\varepsilon(B^+ \rightarrow J/\psi K^+)}{\varepsilon(B_{(s)}^0 \rightarrow e^+e^-)} \times \frac{1}{N(B^+ \rightarrow J/\psi K^+)}, \quad (2)$$

$\varepsilon(B_{(s)}^0 \rightarrow e^+e^-)$ and $\varepsilon(B^+ \rightarrow J/\psi K^+)$ denote the efficiencies of the signal and normalization modes, and $N(B_{(s)}^0 \rightarrow e^+e^-)$ and $N(B^+ \rightarrow J/\psi K^+)$ their yields. The normalization mode branching fraction (including that for the decay $J/\psi \rightarrow e^+e^-$) is $\mathcal{B}(B^+ \rightarrow J/\psi K^+) = (6.03 \pm 0.17) \times 10^{-5}$, taken from Ref. [12]. The b -hadron fragmentation fraction ratio f_d/f_u is assumed to be unity, while $f_s/f_u = 0.259 \pm 0.015$ [32] is used for the Run 1 data and is scaled by 1.068 ± 0.016 for the Run 2 data, according to Ref. [33], to account for center-of-mass energy differences. A measurement of f_s/f_u from Run 2 yields a consistent, but less precise, result [34].

The yield of the normalization mode is determined using an unbinned maximum-likelihood fit to the $K^+e^+e^-$ invariant mass separately for each year of data taking and bremsstrahlung category. The fit model comprises a Gaussian function with power-law tails [35] for the signal component, where the tail parameters are fixed from simulation, and an exponential function to describe combinatorial background. Summed over the bremsstrahlung categories, the yield of the normalization mode is $20\,480 \pm 140$ in the Run 1 data and $33\,080 \pm 180$ in the Run 2 data.

The selection efficiencies $\varepsilon(B_{(s)}^0 \rightarrow e^+e^-)$ and $\varepsilon(B^+ \rightarrow J/\psi K^+)$ are determined separately for each year of data taking and bremsstrahlung category using simulated decays that are weighted to better represent the data. Calibration data are used to evaluate particle-identification efficiencies [25]. Trigger efficiencies are also estimated from data, using the technique described in Ref. [36]. For simulated $B_s^0 \rightarrow e^+e^-$ decays, the mean B_s^0 lifetime [37] is assumed. The selection efficiency is assumed to be the same for both $B^0 \rightarrow e^+e^-$ and $B_s^0 \rightarrow e^+e^-$ decays, which is consistent with results from simulation. The normalization factors, α , are combined across the data-taking periods and given in Table 1, split by bremsstrahlung category (for the selection efficiency ratio between normalization and signal mode, see the Supplemental Material [38]).

In addition to the combinatorial background, backgrounds due to misidentification and partial reconstruction are present in the data. These backgrounds differ significantly between the categories of bremsstrahlung correction. Their invariant-mass shapes and relative contributions are evaluated using simulation. In the lower mass region, partially reconstructed backgrounds of the types $B \rightarrow Xe^+e^-$ and $B^+ \rightarrow \bar{D}^0(\rightarrow Y^+e^-\bar{\nu}_e)e^+\nu_e$ dominate, where X and Y represent hadronic systems. The main source of background in the B -mass region, however, stems from misidentified particles in the decays $B^0 \rightarrow \pi^-e^+\nu_e$ and $B \rightarrow h^+h'^-$, where h and h' are hadrons. The latter has a peaking structure in the B -mass region. Backgrounds involving misidentified particles contribute mostly to categories in which at most one of the electrons has a bremsstrahlung correction applied.

Table 1: Normalization factors α for $B_{(s)}^0 \rightarrow e^+e^-$. The bremsstrahlung category denotes whether zero, one or both electrons are corrected for bremsstrahlung losses. The uncertainties include statistical uncertainties and uncertainties due to limited size of the simulated samples.

Bremsstrahlung category	2011–2012 [10^{-5}]	2015–2016 [10^{-5}]
No correction	2.85 ± 0.24	1.84 ± 0.08
One electron corrected	1.13 ± 0.08	0.70 ± 0.03
Both electrons corrected	1.73 ± 0.20	1.04 ± 0.06

The contribution from combinatorial background is evaluated from same-sign lepton pairs in data and found to be small. The yields of the backgrounds are Gaussian constrained to their expected values, estimated from simulation using their known branching fractions [12].

The shape of the invariant mass of the $B_s^0 \rightarrow e^+e^-$ and $B^0 \rightarrow e^+e^-$ components is modeled using a Gaussian function with power-law tails, where the parameters are obtained from simulation and differ between each bremsstrahlung category and year of data taking. The peak values and the widths of the functions are corrected for data-simulation differences by a factor determined from the normalization mode. The parameters of the $B_s^0 \rightarrow e^+e^-$ and $B^0 \rightarrow e^+e^-$ line shapes are fixed to the same values with the exception of the peak value, which is shifted according to the known B_s^0 – B^0 mass difference [12]. Due to the limited mass resolution, arising from imperfect bremsstrahlung recovery, the line shapes from $B_s^0 \rightarrow e^+e^-$ and $B^0 \rightarrow e^+e^-$ are highly overlapping. Therefore the branching fraction of $B_s^0 \rightarrow e^+e^-$ is obtained by performing a simultaneous fit to the dielectron invariant-mass distribution of all six data sets while neglecting the contribution from $B^0 \rightarrow e^+e^-$, and vice versa. In these fits, the only shared parameters between categories are the branching fractions $\mathcal{B}(B_{(s)}^0 \rightarrow e^+e^-)$ and $\mathcal{B}(B^+ \rightarrow J/\psi K^+)$, and the ratio of the fragmentation fractions f_s/f_u .

Systematic uncertainties are estimated separately for each data set. Dominant sources of systematic uncertainties in the normalization arise from the uncertainty on the fragmentation fraction ratio, the technique used to evaluate the trigger efficiencies, and the determination of particle-identification efficiencies; the systematic uncertainties from these sources extend to 5.8%, 5.3%, and 5.3% on the branching fractions, respectively. The uncertainty on $\mathcal{B}(B^+ \rightarrow J/\psi K^+)$ of 2.8% [12] is taken into account. A difference of up to 4.1% is found between the efficiency of the BDT selection on simulated $B^+ \rightarrow J/\psi K^+$ decays and $B^+ \rightarrow J/\psi K^+$ decays in data, which is assigned as a systematic uncertainty. The fraction of candidates in each bremsstrahlung-correction category of the signal modes is taken from simulation. The difference between simulation and data is investigated using $B^+ \rightarrow J/\psi K^+$ decays and its effect on the normalization, up to 4.0%, is taken as a systematic uncertainty. Systematic uncertainties on the invariant-mass resolution corrections are determined by repeating the correction procedure with pseudoexperiments obtained with the bootstrapping method [39], yielding up to 1.1%. A difference between the total selection efficiencies in the $B_s^0 \rightarrow e^+e^-$ and $B^0 \rightarrow e^+e^-$ channels of up to 2.5% is assigned as a systematic uncertainty on the $B^0 \rightarrow e^+e^-$ normalization factor. Due to the presence of an additional kaon in the final state of the normalization mode, the track-reconstruction efficiency is different between the signal and normalization modes. An uncertainty of 1.1% is assigned to the branching fraction as a systematic uncertainty on

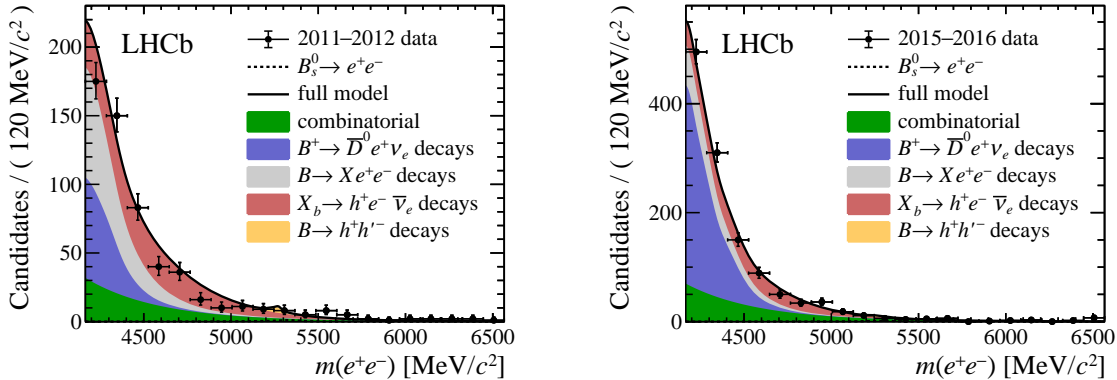


Figure 1: Simultaneous fit to the dielectron invariant-mass distribution, with $\mathcal{B}(B^0 \rightarrow e^+e^-)$ fixed to zero. The sum of bremsstrahlung categories is shown for (left) Run 1 and (right) Run 2. The relative proportions of background contributions change between Run 1 and Run 2 due to different performances of the particle identification algorithms and BDT selections.

the kaon reconstruction efficiency arising from the limited knowledge of the interactions in the detector material [40]. Finally, an uncertainty of 1.0% is assigned to account for small differences in detector occupancy between the signal and normalization mode arising from the trigger selection. The dominant sources of systematic uncertainties on the background composition are due to the imprecise knowledge of the branching fractions of the background components. The largest uncertainty of this type on the expected background yield in the B -mass region is 14%, determined from refitting the mass sidebands while varying the background components according to their uncertainties. Taking all correlations into account, overall single event sensitivities of $[4.71 \pm 0.12(\text{stat.}) \pm 0.33(\text{syst.})] \times 10^{-10}$ for $B_s^0 \rightarrow e^+e^-$ and $[1.271 \pm 0.034(\text{stat.}) \pm 0.063(\text{syst.})] \times 10^{-10}$ for $B^0 \rightarrow e^+e^-$ are obtained.

The dielectron invariant-mass spectrum, summed over bremsstrahlung categories, is shown in Fig. 1, with the result of the $B_s^0 \rightarrow e^+e^-$ fit. The individual categories are shown in the Supplemental Material [38], as well as the distributions with the result of the $B^0 \rightarrow e^+e^-$ fit. The measured branching fractions are $\mathcal{B}(B_s^0 \rightarrow e^+e^-) = (2.4 \pm 4.4) \times 10^{-9}$ and $\mathcal{B}(B^0 \rightarrow e^+e^-) = (0.30 \pm 1.29) \times 10^{-9}$, where the uncertainties include both statistical and systematic components. The results are in agreement with the background-only hypothesis.

Upper limits on the branching fractions are set using the CL_s method [41], as implemented in the GAMMACOMBO framework [42, 43] with a one-sided profile likelihood ratio [44] as test statistic. The likelihoods are computed from fits to the invariant-mass distributions. In the fits, the normalization factor, normalization mode branching fraction, fragmentation fraction ratio, and background yields are Gaussian constrained to their expected values within statistical and systematic uncertainties. Pseudoexperiments, in which the nuisance parameters are set to their fitted values from data, are used for the evaluation of the test statistic.

The expected and observed CL_s distributions are shown in Fig. 2. The upper observed limits are $\mathcal{B}(B_s^0 \rightarrow e^+e^-) < 9.4 (11.2) \times 10^{-9}$ and $\mathcal{B}(B^0 \rightarrow e^+e^-) < 2.5 (3.0) \times 10^{-9}$ at 90 (95)% confidence level. These are consistent with the expected upper limits of $\mathcal{B}(B_s^0 \rightarrow e^+e^-) < 7.0 (8.6) \times 10^{-9}$ and $\mathcal{B}(B^0 \rightarrow e^+e^-) < 2.0 (2.5) \times 10^{-9}$ at 90 (95)% confidence level, obtained as the median of limits determined on background-only pseudoex-

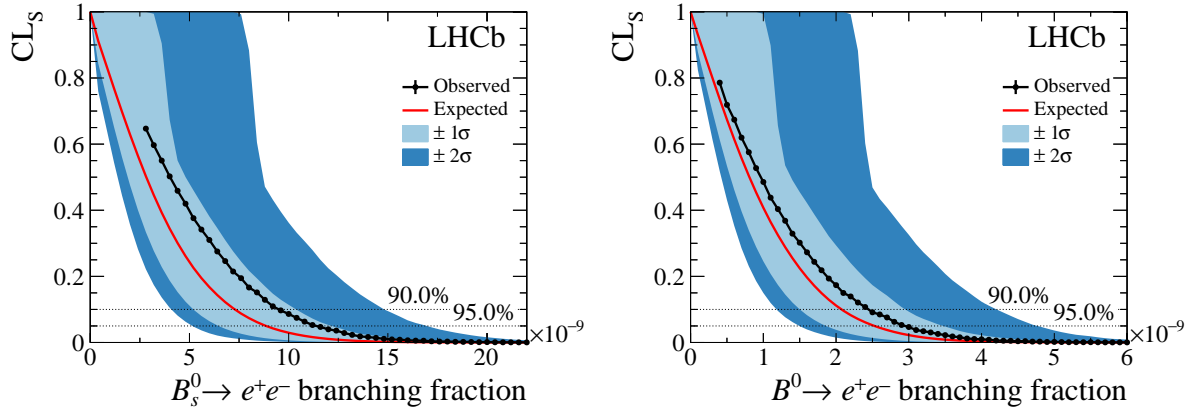


Figure 2: CL_s values as a function of the branching fractions of the decays (left) $B_s^0 \rightarrow e^+e^-$ and (right) $B^0 \rightarrow e^+e^-$. The red solid line (black solid line with data points) corresponds to the distribution of the expected (observed) upper limits, and the light blue (dark blue) band contains the 1σ (2σ) uncertainties on the expected upper limits. Thresholds corresponding to 90% and 95% confidence level are indicated with dashed lines. The observed values are plotted for branching fractions greater than the measured branching fraction in the data; the test statistic is defined to be nonzero only in that region.

periments.

In conclusion, a search for the rare decays $B_{(s)}^0 \rightarrow e^+e^-$ is performed using data from proton-proton collisions recorded with the LHCb experiment, corresponding to a total integrated luminosity of 5 fb^{-1} . No excess of events is observed over the background. The resulting limits on the branching fractions are $\mathcal{B}(B_s^0 \rightarrow e^+e^-) < 9.4 (11.2) \times 10^{-9}$ and $\mathcal{B}(B^0 \rightarrow e^+e^-) < 2.5 (3.0) \times 10^{-9}$ at 90 (95) % confidence level, when neglecting the contribution from the other decay. The mean B_s^0 lifetime is assumed for $B_s^0 \rightarrow e^+e^-$ decays. Assuming SM-like CP -odd (CP -even) $B_s^0 \rightarrow e^+e^-$ decays, an increase (decrease) of 2.4% with respect to the quoted limit is found. The results improve the limits on these branching fractions [11] by more than one order of magnitude and constrain contributions beyond the SM, for example from scalar and pseudoscalar currents [10].

Acknowledgements

We express our gratitude to our colleagues in the CERN accelerator departments for the excellent performance of the LHC. We thank the technical and administrative staff at the LHCb institutes. We acknowledge support from CERN and from the national agencies: CAPES, CNPq, FAPERJ and FINEP (Brazil); MOST and NSFC (China); CNRS/IN2P3 (France); BMBF, DFG and MPG (Germany); INFN (Italy); NWO (Netherlands); MNiSW and NCN (Poland); MEN/IFA (Romania); MSHE (Russia); MinECo (Spain); SNSF and SER (Switzerland); NASU (Ukraine); STFC (United Kingdom); DOE NP and NSF (USA). We acknowledge the computing resources that are provided by CERN, IN2P3 (France), KIT and DESY (Germany), INFN (Italy), SURF (Netherlands), PIC (Spain), GridPP (United Kingdom), RRCKI and Yandex LLC (Russia), CSCS (Switzerland), IFIN-HH (Romania), CBPF (Brazil), PL-GRID (Poland) and OSC (USA). We are indebted to the communities behind the multiple open-source software packages on which we depend.

Individual groups or members have received support from AvH Foundation (Germany); EPLANET, Marie Skłodowska-Curie Actions and ERC (European Union); ANR, Labex P2IO and OCEVU, and Région Auvergne-Rhône-Alpes (France); Key Research Program of Frontier Sciences of CAS, CAS PIFI, and the Thousand Talents Program (China); RFBR, RSF and Yandex LLC (Russia); GVA, XuntaGal and GENCAT (Spain); the Royal Society and the Leverhulme Trust (United Kingdom).

Supplemental Material for LHCb-PAPER-2020-001

The individual categories of the simultaneous fit to the dielectron invariant-mass using the $B_s^0 \rightarrow e^+e^-$ hypothesis are presented in Fig. 3. The fit to the invariant dielectron mass including the $B^0 \rightarrow e^+e^-$ hypothesis instead of the $B_s^0 \rightarrow e^+e^-$ hypothesis is shown in Fig. 4, where the bremsstrahlung categories are summed. The individual categories of the simultaneous fit to the dielectron invariant-mass using the $B^0 \rightarrow e^+e^-$ hypothesis are presented in Fig. 5. Table 2 lists the inputs to the normalization factors: the ratio of normalization and signal efficiencies and the normalization yield. The efficiency of the normalization mode differs from the signal and causes the efficiency ratio to decrease with bremsstrahlung category due to the slightly different reconstruction and preselection and a different impact of the BDT selection, where the differences mainly originate from the additional track in the normalization mode.

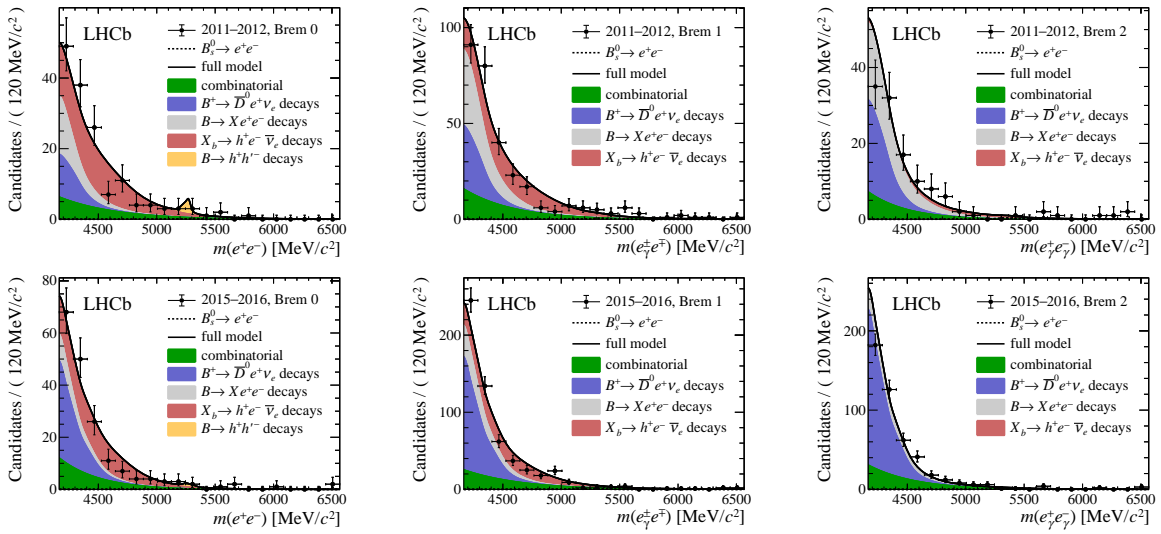


Figure 3: Simultaneous fit to the dielectron invariant-mass distribution in all categories, with $\mathcal{B}(B^0 \rightarrow e^+e^-)$ fixed to zero. The top figures show the three bremsstrahlung categories in the Run 1 data set and the bottom figures show the Run 2 data set. From left to right, the data sets correspond to the bremsstrahlung correction category with no correction, correcting one electron and correcting both electrons. The relative proportions of background contributions change between Run 1 and Run 2 due to different performances of the particle-identification algorithms and BDT selections. Their relative fractions between bremsstrahlung categories follow the expectation from simulation.

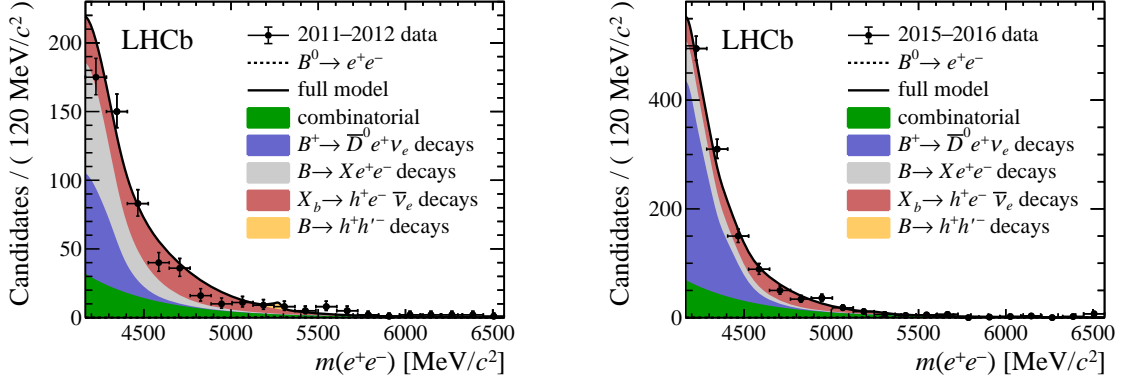


Figure 4: Simultaneous fit to the dielectron invariant-mass distribution, with $\mathcal{B}(B_s^0 \rightarrow e^+e^-)$ fixed to zero. The bremsstrahlung categories are summed over the (left) Run 1 and (right) Run 2 data sets. The relative proportions of background contributions change between Run 1 and Run 2 due to different performances of the particle-identification algorithms and BDT selections.

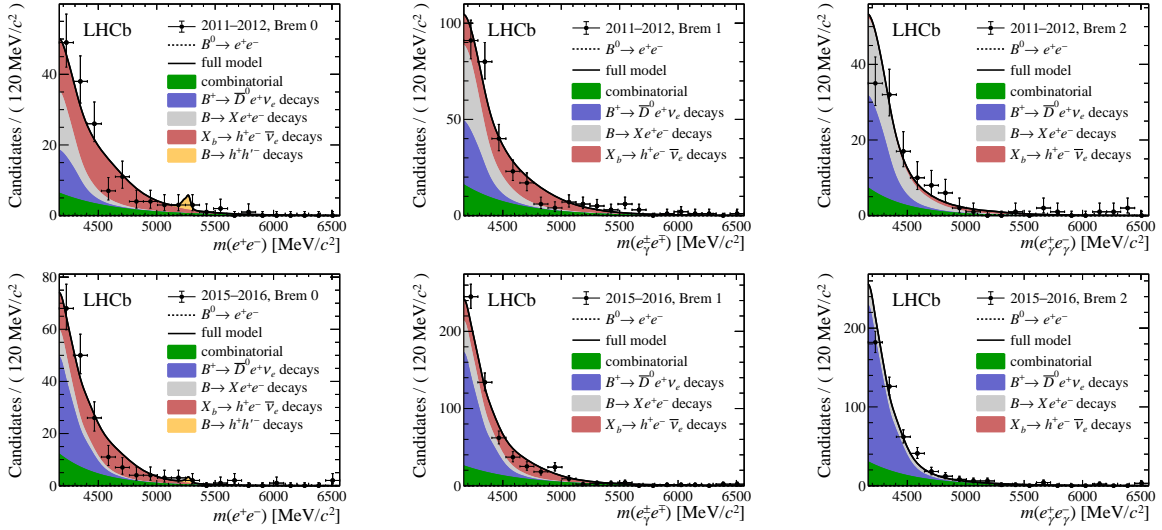


Figure 5: Simultaneous fit to the dielectron invariant-mass distribution in all categories, with $\mathcal{B}(B_s^0 \rightarrow e^+e^-)$ fixed to zero. The top figures show the three bremsstrahlung categories in the Run 1 data set and the bottom figures show the Run 2 data set. From left to right, the data sets correspond to the bremsstrahlung correction category with no correction, correcting one electron and correcting both electrons. The relative proportions of background contributions change between Run 1 and Run 2 due to different performances of the particle-identification algorithms and BDT selections. Their relative fractions between bremsstrahlung categories follow the expectation from simulation.

Table 2: Inputs for the normalization factors, the efficiency ratio $\varepsilon(B^+ \rightarrow J/\psi K^+)/\varepsilon(B_{(s)}^0 \rightarrow e^+e^-)$ and normalization yield $N(B^+ \rightarrow J/\psi K^+)$. The bremsstrahlung category (Brem. cat.) denotes whether zero, one or both electrons are corrected for bremsstrahlung losses. The uncertainties on the efficiency ratios include statistical uncertainties from the calibration and uncertainties due to limited size of the simulated samples.

Brem. cat.	2011–2012		2015–2016	
	Efficiency ratio	Norm. yield [10^3]	Efficiency ratio	Norm. yield [10^3]
Brem. 0	0.144 ± 0.012	5.05 ± 0.07	0.148 ± 0.118	7.96 ± 0.09
Brem. 1	0.119 ± 0.008	10.43 ± 0.11	0.118 ± 0.005	12.75 ± 0.05
Brem. 2	0.086 ± 0.010	4.95 ± 0.07	0.085 ± 0.005	8.306 ± 0.032

References

- [1] LHCb collaboration, R. Aaij *et al.*, *Test of lepton universality with $B^0 \rightarrow K^{*0} \ell^+ \ell^-$ decays*, JHEP **08** (2017) 055, [arXiv:1705.05802](#).
- [2] LHCb collaboration, R. Aaij *et al.*, *Search for lepton-universality violation in $B^+ \rightarrow K^+ \ell^+ \ell^-$ decays*, Phys. Rev. Lett. **122** (2019) 191801, [arXiv:1903.09252](#).
- [3] LHCb collaboration, R. Aaij *et al.*, *Test of lepton universality using $\Lambda_b^0 \rightarrow p K^- \ell^+ \ell^-$ decays*, JHEP **05** (2020) 040, [arXiv:1912.08139](#).
- [4] BaBar collaboration, J. P. Lees *et al.*, *Measurement of branching fractions and rate asymmetries in the rare decays $B \rightarrow K^{(*)} \ell^+ \ell^-$* , Phys. Rev. **D86** (2012) 032012, [arXiv:1204.3933](#).
- [5] Belle collaboration, A. Abdesselam *et al.*, *Test of lepton flavor universality in $B \rightarrow K \ell^+ \ell^-$ decays*, [arXiv:1908.01848](#).
- [6] Belle collaboration, A. Abdesselam *et al.*, *Test of lepton flavor universality in $B \rightarrow K^* \ell^+ \ell^-$ decays at Belle*, [arXiv:1904.02440](#).
- [7] CMS and LHCb collaborations, V. Khachatryan *et al.*, *Observation of the rare $B_s^0 \rightarrow \mu^+ \mu^-$ decay from the combined analysis of CMS and LHCb data*, Nature **522** (2015) 68, [arXiv:1411.4413](#).
- [8] LHCb collaboration, R. Aaij *et al.*, *Measurement of the $B_s^0 \rightarrow \mu^+ \mu^-$ branching fraction and effective lifetime and search for $B^0 \rightarrow \mu^+ \mu^-$ decays*, Phys. Rev. Lett. **118** (2017) 191801, [arXiv:1703.05747](#).
- [9] M. Beneke, C. Bobeth, and R. Szafron, *Power-enhanced leading-logarithmic QED corrections to $B_q \rightarrow \mu^+ \mu^-$* , JHEP **10** (2019) 232, [arXiv:1908.07011](#).
- [10] R. Fleischer, R. Jaarsma, and G. Tetlalmatzi-Xolocotzi, *In pursuit of New Physics with $B_{s,d}^0 \rightarrow \ell^+ \ell^-$* , JHEP **05** (2017) 156, [arXiv:1703.10160](#).
- [11] CDF collaboration, T. Aaltonen *et al.*, *Search for the decays $B_s^0 \rightarrow e^+ \mu^-$ and $B_s^0 \rightarrow e^+ e^-$ in CDF Run II*, Phys. Rev. Lett. **102** (2009) 201801, [arXiv:0901.3803](#).
- [12] Particle Data Group, M. Tanabashi *et al.*, *Review of particle physics*, Phys. Rev. **D98** (2018) 030001, and 2019 update.
- [13] LHCb collaboration, A. A. Alves Jr. *et al.*, *The LHCb detector at the LHC*, JINST **3** (2008) S08005.
- [14] LHCb collaboration, R. Aaij *et al.*, *LHCb detector performance*, Int. J. Mod. Phys. **A30** (2015) 1530022, [arXiv:1412.6352](#).
- [15] R. Aaij *et al.*, *The LHCb trigger and its performance in 2011*, JINST **8** (2013) P04022, [arXiv:1211.3055](#).
- [16] V. V. Gligorov and M. Williams, *Efficient, reliable and fast high-level triggering using a bonsai boosted decision tree*, JINST **8** (2013) P02013, [arXiv:1210.6861](#).

- [17] T. Likhomanenko *et al.*, *LHCb topological trigger reoptimization*, J. Phys. Conf. Ser. **664** (2015) 082025.
- [18] T. Sjöstrand, S. Mrenna, and P. Skands, *PYTHIA 6.4 physics and manual*, JHEP **05** (2006) 026, [arXiv:hep-ph/0603175](#); T. Sjöstrand, S. Mrenna, and P. Skands, *A brief introduction to PYTHIA 8.1*, Comput. Phys. Commun. **178** (2008) 852, [arXiv:0710.3820](#).
- [19] I. Belyaev *et al.*, *Handling of the generation of primary events in Gauss, the LHCb simulation framework*, J. Phys. Conf. Ser. **331** (2011) 032047.
- [20] D. J. Lange, *The EvtGen particle decay simulation package*, Nucl. Instrum. Meth. **A462** (2001) 152.
- [21] P. Golonka and Z. Was, *PHOTOS Monte Carlo: A precision tool for QED corrections in Z and W decays*, Eur. Phys. J. **C45** (2006) 97, [arXiv:hep-ph/0506026](#).
- [22] Geant4 collaboration, J. Allison *et al.*, *Geant4 developments and applications*, IEEE Trans. Nucl. Sci. **53** (2006) 270; Geant4 collaboration, S. Agostinelli *et al.*, *Geant4: A simulation toolkit*, Nucl. Instrum. Meth. **A506** (2003) 250.
- [23] M. Clemencic *et al.*, *The LHCb simulation application, Gauss: Design, evolution and experience*, J. Phys. Conf. Ser. **331** (2011) 032023.
- [24] LHCb collaboration, R. Aaij *et al.*, *Search for the rare decays $B_s^0 \rightarrow \mu^+ \mu^-$ and $B^0 \rightarrow \mu^+ \mu^-$* , Phys. Lett. **B708** (2012) 55, [arXiv:1112.1600](#).
- [25] L. Anderlini *et al.*, *The PIDCalib package*, LHCb-PUB-2016-021, 2016.
- [26] LHCb collaboration, R. Aaij *et al.*, *Measurement of the $B^0 \rightarrow K^{*0} e^+ e^-$ branching fraction at low dilepton mass*, JHEP **05** (2013) 159, [arXiv:1304.3035](#).
- [27] Y. Freund and R. E. Schapire, *A decision-theoretic generalization of on-line learning and an application to boosting*, J. Comput. Syst. Sci. **55** (1997) 119.
- [28] L. Breiman, J. H. Friedman, R. A. Olshen, and C. J. Stone, *Classification and regression trees*, Wadsworth international group, Belmont, California, USA, 1984.
- [29] F. Pedregosa *et al.*, *Scikit-learn: Machine learning in Python*, J. Machine Learning Res. **12** (2011) 2825, [arXiv:1201.0490](#), and online at <http://scikit-learn.org/stable/>.
- [30] L. Gavardi, *Search for lepton flavour violation in τ decays at the LHCb experiment*, Master's thesis, Universit degli studi di Milano-Bicocca, 2013, presented 28 Nov 2013, CERN-THESIS-2013-259.
- [31] G. Punzi, *Sensitivity of searches for new signals and its optimization*, eConf **C030908** (2003) MODT002, [arXiv:physics/0308063](#).
- [32] LHCb collaboration, R. Aaij *et al.*, *Measurement of the fragmentation fraction ratio f_s/f_d and its dependence on B meson kinematics*, JHEP **04** (2013) 001, [arXiv:1301.5286](#), f_s/f_d value updated in LHCb-CONF-2013-011.

- [33] LHCb collaboration, R. Aaij *et al.*, *Measurement of f_s/f_u variation with proton-proton collision energy and B -meson kinematics*, Phys. Rev. Lett. **124** (2020) 122002, [arXiv:1910.09934](#).
- [34] LHCb collaboration, R. Aaij *et al.*, *Measurement of b -hadron fractions in 13 TeV pp collisions*, Phys. Rev. **D100** (2019) 031102(R), [arXiv:1902.06794](#).
- [35] T. Skwarnicki, *A study of the radiative cascade transitions between the Upsilon-prime and Upsilon resonances*, PhD thesis, Institute of Nuclear Physics, Krakow, 1986, DESY-F31-86-02.
- [36] S. Tolk, J. Albrecht, F. Dettori, and A. Pellegrino, *Data driven trigger efficiency determination at LHCb*, LHCb-PUB-2014-039, 2014.
- [37] Particle Data Group, K. A. Olive *et al.*, *Review of particle physics*, Chin. Phys. **C38** (2014) 090001.
- [38] See Supplemental Material for the selection efficiency ratio of normalization and signal mode, the individual categories of the $B_s^0 \rightarrow e^+e^-$ fit and the distributions with the result of the $B^0 \rightarrow e^+e^-$ fit.
- [39] B. Efron and R. J. Tibshirani, *An introduction to the bootstrap*, Mono. Stat. Appl. Probab., Chapman and Hall, London, 1993.
- [40] LHCb collaboration, R. Aaij *et al.*, *Measurement of the track reconstruction efficiency at LHCb*, JINST **10** (2015) P02007, [arXiv:1408.1251](#).
- [41] A. L. Read, *Presentation of search results: The CL_s technique*, J. Phys. **G28** (2002) 2693.
- [42] LHCb collaboration, R. Aaij *et al.*, *Measurement of the CKM angle γ from a combination of LHCb results*, JHEP **12** (2016) 087, [arXiv:1611.03076](#).
- [43] M. Kenzie *et al.*, *GammaCombo: A statistical analysis framework for combining measurements, fitting datasets and producing confidence intervals*, doi: 10.5281/zenodo.3371421.
- [44] G. Cowan, K. Cranmer, E. Gross, and O. Vitells, *Asymptotic formulae for likelihood-based tests of new physics*, Eur. Phys. J. **C71** (2011) 1554, Erratum *ibid.* **C73** (2013) 2501, [arXiv:1007.1727](#).

LHCb collaboration

R. Aaij³¹, C. Abellán Beteta⁴⁹, T. Ackernley⁵⁹, B. Adeva⁴⁵, M. Adinolfi⁵³, H. Afsharnia⁹, C.A. Aidala⁸¹, S. Aiola²⁵, Z. Ajaltouni⁹, S. Akar⁶⁶, P. Albicocco²², J. Albrecht¹⁴, F. Alessio⁴⁷, M. Alexander⁵⁸, A. Alfonso Alberio⁴⁴, G. Alkhazov³⁷, P. Alvarez Cartelle⁶⁰, A.A. Alves Jr⁴⁵, S. Amato², Y. Amhis¹¹, L. An²¹, L. Anderlini²¹, G. Andreassi⁴⁸, M. Andreotti²⁰, F. Archilli¹⁶, A. Artamonov⁴³, M. Artuso⁶⁷, K. Arzymatov⁴¹, E. Aslanides¹⁰, M. Atzeni⁴⁹, B. Audurier¹¹, S. Bachmann¹⁶, J.J. Back⁵⁵, S. Baker⁶⁰, V. Balagura^{11,b}, W. Baldini²⁰, A. Baranov⁴¹, R.J. Barlow⁶¹, S. Barsuk¹¹, W. Barter⁶⁰, M. Bartolini^{23,47,h}, F. Baryshnikov⁷⁸, J.M. Basels¹³, G. Bassi²⁸, V. Batozskaya³⁵, B. Batsukh⁶⁷, A. Battig¹⁴, A. Bay⁴⁸, M. Becker¹⁴, F. Bedeschi²⁸, I. Bediaga¹, A. Beiter⁶⁷, V. Belavin⁴¹, S. Belin²⁶, V. Bellec⁴⁸, K. Belous⁴³, I. Belyaev³⁸, G. Bencivenni²², E. Ben-Haim¹², S. Benson³¹, A. Berezhnoy³⁹, R. Bernet⁴⁹, D. Berninghoff¹⁶, H.C. Bernstein⁶⁷, C. Bertella⁴⁷, E. Bertholet¹², A. Bertolin²⁷, C. Betancourt⁴⁹, F. Betti^{19,e}, M.O. Bettler⁵⁴, I.a. Bezshyiko⁴⁹, S. Bhasin⁵³, J. Bhom³³, M.S. Bieker¹⁴, S. Bifani⁵², P. Billoir¹², A. Bizzeti^{21,t}, M. Bjørn⁶², M.P. Blago⁴⁷, T. Blake⁵⁵, F. Blanc⁴⁸, S. Blusk⁶⁷, D. Bobulska⁵⁸, V. Bocci³⁰, O. Boente Garcia⁴⁵, T. Boettcher⁶³, A. Boldyrev⁷⁹, A. Bondar^{42,w}, N. Bondar^{37,47}, S. Borghi⁶¹, M. Borisyak⁴¹, M. Borsato¹⁶, J.T. Borsuk³³, T.J.V. Bowcock⁵⁹, C. Bozzi²⁰, M.J. Bradley⁶⁰, S. Braun⁶⁵, A. Brea Rodriguez⁴⁵, M. Brodski⁴⁷, J. Brodzicka³³, A. Brossa Gonzalo⁵⁵, D. Brundu²⁶, E. Buchanan⁵³, A. Büchler-Germann⁴⁹, A. Buonauro⁴⁹, C. Burr⁴⁷, A. Bursche²⁶, A. Butkevich⁴⁰, J.S. Butter³¹, J. Buytaert⁴⁷, W. Byczynski⁴⁷, S. Cadeddu²⁶, H. Cai⁷², R. Calabrese^{20,g}, L. Calero Diaz²², S. Cali²², R. Calladine⁵², M. Calvi^{24,i}, M. Calvo Gomez^{44,l}, P. Camargo Magalhaes⁵³, A. Camboni^{44,l}, P. Campana²², D.H. Campora Perez³¹, A.F. Campoverde Quezada⁵, L. Capriotti^{19,e}, A. Carbone^{19,e}, G. Carboni²⁹, R. Cardinale^{23,h}, A. Cardini²⁶, I. Carli⁶, P. Carniti^{24,i}, K. Carvalho Akiba³¹, A. Casais Vidal⁴⁵, G. Casse⁵⁹, M. Cattaneo⁴⁷, G. Cavallero⁴⁷, S. Celani⁴⁸, R. Cenci^{28,o}, J. Cerasoli¹⁰, M.G. Chapman⁵³, M. Charles¹², Ph. Charpentier⁴⁷, G. Chatzikonstantinidis⁵², M. Chefdeville⁸, V. Chekalina⁴¹, C. Chen³, S. Chen²⁶, A. Chernov³³, S.-G. Chitic⁴⁷, V. Chobanova⁴⁵, S. Cholak⁴⁸, M. Chruszcz³³, A. Chubykin³⁷, V. Chulikov³⁷, P. Ciambrone²², M.F. Cicala⁵⁵, X. Cid Vidal⁴⁵, G. Ciezarek⁴⁷, F. Cindolo¹⁹, P.E.L. Clarke⁵⁷, M. Clemencic⁴⁷, H.V. Cliff⁵⁴, J. Closier⁴⁷, J.L. Cobbedick⁶¹, V. Coco⁴⁷, J.A.B. Coelho¹¹, J. Cogan¹⁰, E. Cogneras⁹, L. Cojocariu³⁶, P. Collins⁴⁷, T. Colombo⁴⁷, A. Contu²⁶, N. Cooke⁵², G. Coombs⁵⁸, S. Coquereau⁴⁴, G. Corti⁴⁷, C.M. Costa Sobral⁵⁵, B. Couturier⁴⁷, D.C. Craik⁶³, J. Crkovská⁶⁶, A. Crocombe⁵⁵, M. Cruz Torres^{1,z}, R. Currie⁵⁷, C.L. Da Silva⁶⁶, E. Dall'Occo¹⁴, J. Dalseno^{45,53}, C. D'Ambrosio⁴⁷, A. Danilina³⁸, P. d'Argent⁴⁷, A. Davis⁶¹, O. De Aguiar Francisco⁴⁷, K. De Bruyn⁴⁷, S. De Capua⁶¹, M. De Cian⁴⁸, J.M. De Miranda¹, L. De Paula², M. De Serio^{18,d}, P. De Simone²², J.A. de Vries⁷⁶, C.T. Dean⁶⁶, W. Dean⁸¹, D. Decamp⁸, L. Del Buono¹², B. Delaney⁵⁴, H.-P. Dembinski¹⁴, A. Dendek³⁴, V. Denysenko⁴⁹, D. Derkach⁷⁹, O. Deschamps⁹, F. Desse¹¹, F. Dettori^{26,f}, B. Dey⁷, A. Di Canto⁴⁷, P. Di Nezza²², S. Didenko⁷⁸, H. Dijkstra⁴⁷, V. Dobishuk⁵¹, F. Dordei²⁶, M. Dorigo^{28,x}, A.C. dos Reis¹, L. Douglas⁵⁸, A. Dovbnya⁵⁰, K. Dreimanis⁵⁹, M.W. Dudek³³, L. Dufour⁴⁷, P. Durante⁴⁷, J.M. Durham⁶⁶, D. Dutta⁶¹, M. Dziewiecki¹⁶, A. Dziurda³³, A. Dzyuba³⁷, S. Easo⁵⁶, U. Egede⁶⁹, V. Egorychev³⁸, S. Eidelman^{42,w}, S. Eisenhardt⁵⁷, S. Ek-In⁴⁸, L. Eklund⁵⁸, S. Ely⁶⁷, A. Ene³⁶, E. Epple⁶⁶, S. Escher¹³, J. Eschle⁴⁹, S. Esen³¹, T. Evans⁴⁷, A. Falabella¹⁹, J. Fan³, Y. Fan⁵, N. Farley⁵², S. Farry⁵⁹, D. Fazzini¹¹, P. Fedin³⁸, M. Féo⁴⁷, P. Fernandez Declara⁴⁷, A. Fernandez Prieto⁴⁵, F. Ferrari^{19,e}, L. Ferreira Lopes⁴⁸, F. Ferreira Rodrigues², S. Ferreres Sole³¹, M. Ferrillo⁴⁹, M. Ferro-Luzzi⁴⁷, S. Filippov⁴⁰, R.A. Fini¹⁸, M. Fiorini^{20,g}, M. Firlej³⁴, K.M. Fischer⁶², C. Fitzpatrick⁴⁷, T. Fiutowski³⁴, F. Fleuret^{11,b}, M. Fontana⁴⁷, F. Fontanelli^{23,h}, R. Forty⁴⁷, V. Franco Lima⁵⁹, M. Franco Sevilla⁶⁵, M. Frank⁴⁷, C. Frei⁴⁷, D.A. Friday⁵⁸, J. Fu^{25,p}, Q. Fuehring¹⁴, W. Funk⁴⁷, E. Gabriel⁵⁷, A. Gallas Torreira⁴⁵, D. Galli^{19,e}, S. Gallorini²⁷, S. Gambetta⁵⁷, Y. Gan³, M. Gandelman², P. Gandini²⁵, Y. Gao⁴,

L.M. Garcia Martin⁴⁶, J. García Pardiñas⁴⁹, B. Garcia Plana⁴⁵, F.A. Garcia Rosales¹¹,
 L. Garrido⁴⁴, D. Gascon⁴⁴, C. Gaspar⁴⁷, D. Gerick¹⁶, E. Gersabeck⁶¹, M. Gersabeck⁶¹,
 T. Gershon⁵⁵, D. Gerstel¹⁰, Ph. Ghez⁸, V. Gibson⁵⁴, A. Gioventù⁴⁵, P. Gironella Gironell⁴⁴,
 L. Giubega³⁶, C. Giugliano²⁰, K. Gizdov⁵⁷, V.V. Gligorov¹², C. Göbel⁷⁰, E. Golobardes^{44,l},
 D. Golubkov³⁸, A. Golutvin^{60,78}, A. Gomes^{1,a}, P. Gorbounov³⁸, I.V. Gorelov³⁹, C. Gotti^{24,i},
 E. Govorkova³¹, J.P. Grabowski¹⁶, R. Graciani Diaz⁴⁴, T. Grammatico¹²,
 L.A. Granado Cardoso⁴⁷, E. Graugés⁴⁴, E. Graverini⁴⁸, G. Graziani²¹, A. Grecu³⁶, R. Greim³¹,
 P. Griffith²⁰, L. Grillo⁶¹, L. Gruber⁴⁷, B.R. Gruberg Cazon⁶², C. Gu³, E. Gushchin⁴⁰,
 A. Guth¹³, Yu. Guz^{43,47}, T. Gys⁴⁷, P. A. Gnther¹⁶, T. Hadavizadeh⁶², G. Haefeli⁴⁸, C. Haen⁴⁷,
 S.C. Haines⁵⁴, P.M. Hamilton⁶⁵, Q. Han⁷, X. Han¹⁶, T.H. Hancock⁶², S. Hansmann-Menzemer¹⁶,
 N. Harnew⁶², T. Harrison⁵⁹, R. Hart³¹, C. Hasse¹⁴, M. Hatch⁴⁷, J. He⁵, M. Hecker⁶⁰,
 K. Heijhoff³¹, K. Heinicke¹⁴, A.M. Hennequin⁴⁷, K. Hennessy⁵⁹, L. Henry⁴⁶, J. Heuel¹³,
 A. Hicheur⁶⁸, D. Hill⁶², M. Hilton⁶¹, P.H. Hopchev⁴⁸, J. Hu¹⁶, J. Hu⁷¹, W. Hu⁷, W. Huang⁵,
 W. Hulsbergen³¹, T. Humair⁶⁰, R.J. Hunter⁵⁵, M. Hushchyn⁷⁹, D. Hutchcroft⁵⁹, D. Hynds³¹,
 P. Ibis¹⁴, M. Idzik³⁴, P. Ilten⁵², A. Inglese³⁷, K. Ivshin³⁷, R. Jacobsson⁴⁷, S. Jakobsen⁴⁷,
 E. Jans³¹, B.K. Jashal⁴⁶, A. Jawahery⁶⁵, V. Jevtic¹⁴, F. Jiang³, M. John⁶², D. Johnson⁴⁷,
 C.R. Jones⁵⁴, B. Jost⁴⁷, N. Jurik⁶², S. Kandybei⁵⁰, M. Karacson⁴⁷, J.M. Kariuki⁵³, N. Kazeev⁷⁹,
 M. Kecke¹⁶, F. Keizer^{54,47}, M. Kelsey⁶⁷, M. Kenzie⁵⁵, T. Ketel³², B. Khanji⁴⁷, A. Kharisova⁸⁰,
 K.E. Kim⁶⁷, T. Kirn¹³, V.S. Kirsbaum⁴⁸, S. Klaver²², K. Klimaszewski³⁵, S. Koliiev⁵¹,
 A. Kondybayeva⁷⁸, A. Konoplyannikov³⁸, P. Kopciwicz³⁴, R. Kopecna¹⁶, P. Koppenburg³¹,
 M. Korolev³⁹, I. Kostiuik^{31,51}, O. Kot⁵¹, S. Kotriakhova³⁷, L. Kravchuk⁴⁰, R.D. Krawczyk⁴⁷,
 M. Kreps⁵⁵, F. Kress⁶⁰, S. Kretzschmar¹³, P. Krokovny^{42,w}, W. Krupa³⁴, W. Krzemien³⁵,
 W. Kucewicz^{33,k}, M. Kucharczyk³³, V. Kudryavtsev^{42,w}, H.S. Kuindersma³¹, G.J. Kunde⁶⁶,
 T. Kvaratskheliya³⁸, D. Lacarrere⁴⁷, G. Lafferty⁶¹, A. Lai²⁶, D. Lancierini⁴⁹, J.J. Lane⁶¹,
 G. Lanfranchi²², C. Langenbruch¹³, O. Lantwin⁴⁹, T. Latham⁵⁵, F. Lazzari^{28,u}, R. Le Gac¹⁰,
 S.H. Lee⁸¹, R. Lefèvre⁹, A. Leflat^{39,47}, O. Leroy¹⁰, T. Lesiak³³, B. Leverington¹⁶, H. Li⁷¹,
 L. Li⁶², X. Li⁶⁶, Y. Li⁶, Z. Li⁶⁷, X. Liang⁶⁷, T. Lin⁶⁰, R. Lindner⁴⁷, V. Lisovskyi¹⁴, G. Liu⁷¹,
 X. Liu³, D. Loh⁵⁵, A. Loi²⁶, J. Lomba Castro⁴⁵, I. Longstaff⁵⁸, J.H. Lopes², G. Loustau⁴⁹,
 G.H. Lovell⁵⁴, Y. Lu⁶, D. Lucchesi^{27,n}, M. Lucio Martinez³¹, Y. Luo³, A. Lupato²⁷, E. Luppi^{20,g},
 O. Lupton⁵⁵, A. Lusiani^{28,s}, X. Lyu⁵, S. Maccolini^{19,e}, F. Machefer¹¹, F. Maciuc³⁶, V. Macko⁴⁸,
 P. Mackowiak¹⁴, S. Maddrell-Mander⁵³, L.R. Madhan Mohan⁵³, O. Maev³⁷, A. Maevskiy⁷⁹,
 D. Maisuzenko³⁷, M.W. Majewski³⁴, S. Malde⁶², B. Malecki⁴⁷, A. Malinin⁷⁷, T. Maltsev^{42,w},
 H. Malygina¹⁶, G. Manca^{26,f}, G. Mancinelli¹⁰, R. Manera Escalero⁴⁴, D. Manuzzi^{19,e},
 D. Marangotto^{25,p}, J. Maratas^{9,v}, J.F. Marchand⁸, U. Marconi¹⁹, S. Mariani^{21,21,47},
 C. Marin Benito¹¹, M. Marinangeli⁴⁸, P. Marino⁴⁸, J. Marks¹⁶, P.J. Marshall⁵⁹, G. Martellotti³⁰,
 L. Martinazzoli⁴⁷, M. Martinelli^{24,i}, D. Martinez Santos⁴⁵, F. Martinez Vidal⁴⁶, A. Massafferri¹,
 M. Materok¹³, R. Matev⁴⁷, A. Mathad⁴⁹, Z. Mathe⁴⁷, V. Matiunin³⁸, C. Matteuzzi²⁴,
 K.R. Mattioli⁸¹, A. Mauri⁴⁹, E. Maurice^{11,b}, M. McCann⁶⁰, L. McConnell¹⁷, A. McNab⁶¹,
 R. McNulty¹⁷, J.V. Mead⁵⁹, B. Meadows⁶⁴, C. Meaux¹⁰, G. Meier¹⁴, N. Meinert⁷⁴,
 D. Melnychuk³⁵, S. Meloni^{24,i}, M. Merk³¹, A. Merli²⁵, M. Mikhasenko⁴⁷, D.A. Milanese⁷³,
 E. Millard⁵⁵, M.-N. Minard⁸, O. Mineev³⁸, L. Minzoni²⁰, S.E. Mitchell⁵⁷, B. Mitreska⁶¹,
 D.S. Mitzel⁴⁷, A. Mödden¹⁴, A. Mogini¹², R.D. Moise⁶⁰, T. Mombächer¹⁴, I.A. Monroy⁷³,
 S. Monteil⁹, M. Morandin²⁷, G. Morello²², M.J. Morello^{28,s}, J. Moron³⁴, A.B. Morris¹⁰,
 A.G. Morris⁵⁵, R. Mountain⁶⁷, H. Mu³, F. Muheim⁵⁷, M. Mukherjee⁷, M. Mulder⁴⁷,
 D. Müller⁴⁷, K. Müller⁴⁹, C.H. Murphy⁶², D. Murray⁶¹, P. Muzzetto²⁶, P. Naik⁵³, T. Nakada⁴⁸,
 R. Nandakumar⁵⁶, T. Nanut⁴⁸, I. Nasteva², M. Needham⁵⁷, N. Neri^{25,p}, S. Neubert¹⁶,
 N. Neufeld⁴⁷, R. Newcombe⁶⁰, T.D. Nguyen⁴⁸, C. Nguyen-Mau^{48,m}, E.M. Niel¹¹, S. Nieswand¹³,
 N. Nikitin³⁹, N.S. Nolte⁴⁷, C. Nunez⁸¹, A. Oblakowska-Mucha³⁴, V. Obraztsov⁴³, S. Ogilvy⁵⁸,
 D.P. O'Hanlon⁵³, R. Oldeman^{26,f}, C.J.G. Onderwater⁷⁵, J. D. Osborn⁸¹, A. Ossowska³³,
 J.M. Otalora Goicochea², T. Ovsiannikova³⁸, P. Owen⁴⁹, A. Oyanguren⁴⁶, P.R. Pais⁴⁸,

T. Pajero^{28,28,47,s}, A. Palano¹⁸, M. Palutan²², G. Panshin⁸⁰, A. Papanestis⁵⁶, M. Pappagallo⁵⁷,
 L.L. Pappalardo²⁰, C. Pappenheimer⁶⁴, W. Parker⁶⁵, C. Parkes⁶¹, G. Passaleva^{21,47},
 A. Pastore¹⁸, M. Patel⁶⁰, C. Patrignani^{19,e}, A. Pearce⁴⁷, A. Pellegrino³¹, M. Pepe Altarelli⁴⁷,
 S. Perazzini¹⁹, D. Pereima³⁸, P. Perret⁹, L. Pescatore⁴⁸, K. Petridis⁵³, A. Petrolini^{23,h},
 A. Petrov⁷⁷, S. Petrucci⁵⁷, M. Petruzzo^{25,p}, B. Pietrzyk⁸, G. Pietrzyk⁴⁸, M. Pili⁶², D. Pinci³⁰,
 J. Pinzino⁴⁷, F. Pisani¹⁹, A. Piucci¹⁶, V. Placinta³⁶, S. Playfer⁵⁷, J. Plews⁵², M. Plo Casasus⁴⁵,
 F. Polci¹², M. Poli Lener²², M. Poliakov⁶⁷, A. Poluektov¹⁰, N. Polukhina^{78,c}, I. Polyakov⁶⁷,
 E. Polycarpo², G.J. Pomery⁵³, S. Ponce⁴⁷, A. Popov⁴³, D. Popov⁵², S. Poslavskii⁴³,
 K. Prasanth³³, L. Promberger⁴⁷, C. Prouve⁴⁵, V. Pugatch⁵¹, A. Puig Navarro⁴⁹, H. Pullen⁶²,
 G. Punzi^{28,o}, W. Qian⁵, J. Qin⁵, R. Quagliani¹², B. Quintana⁸, N.V. Raab¹⁷,
 R.I. Rabadan Trejo¹⁰, B. Rachwal³⁴, J.H. Rademacker⁵³, M. Rama²⁸, M. Ramos Pernas⁴⁵,
 M.S. Rangel², F. Ratnikov^{41,79}, G. Raven³², M. Reboud⁸, F. Redi⁴⁸, F. Reiss¹²,
 C. Remon Alepuz⁴⁶, Z. Ren³, V. Renaudin⁶², S. Ricciardi⁵⁶, D.S. Richards⁵⁶, S. Richards⁵³,
 K. Rinnert⁵⁹, P. Robbe¹¹, A. Robert¹², A.B. Rodrigues⁴⁸, E. Rodrigues⁵⁹,
 J.A. Rodriguez Lopez⁷³, M. Roehrken⁴⁷, A. Rollings⁶², V. Romanovskiy⁴³, M. Romero Lamas⁴⁵,
 A. Romero Vidal⁴⁵, J.D. Roth⁸¹, M. Rotondo²², M.S. Rudolph⁶⁷, T. Ruf⁴⁷, J. Ruiz Vidal⁴⁶,
 A. Ryzhikov⁷⁹, J. Ryzka³⁴, J.J. Saborido Silva⁴⁵, N. Sagidova³⁷, N. Sahoo⁵⁵, B. Saitta^{26,f},
 C. Sanchez Gras³¹, C. Sanchez Mayordomo⁴⁶, R. Santacesaria³⁰, C. Santamarina Rios⁴⁵,
 M. Santimaria²², E. Santovetti^{29,j}, G. Sarpis⁶¹, M. Sarpis¹⁶, A. Sarti³⁰, C. Satriano^{30,r},
 A. Satta²⁹, M. Saur⁵, D. Savrina^{38,39}, L.G. Scantlebury Smead⁶², S. Schael¹³, M. Schellenberg¹⁴,
 M. Schiller⁵⁸, H. Schindler⁴⁷, M. Schmelling¹⁵, T. Schmelzer¹⁴, B. Schmidt⁴⁷, O. Schneider⁴⁸,
 A. Schopper⁴⁷, H.F. Schreiner⁶⁴, M. Schubiger³¹, S. Schulte⁴⁸, M.H. Schune¹¹, R. Schwemmer⁴⁷,
 B. Sciascia²², A. Sciubba²², S. Sellam⁶⁸, A. Semennikov³⁸, A. Sergi^{52,47}, N. Serra⁴⁹,
 J. Serrano¹⁰, L. Sestini²⁷, A. Seuthe¹⁴, P. Seyfert⁴⁷, D.M. Shangase⁸¹, M. Shapkin⁴³,
 L. Shchutka⁴⁸, T. Shears⁵⁹, L. Shekhtman^{42,w}, V. Shevchenko⁷⁷, E. Shmanin⁷⁸,
 J.D. Shupperd⁶⁷, B.G. Siddi²⁰, R. Silva Coutinho⁴⁹, L. Silva de Oliveira², G. Simi^{27,n},
 S. Simone^{18,d}, I. Skiba²⁰, N. Skidmore¹⁶, T. Skwarnicki⁶⁷, M.W. Slater⁵², J.G. Smeaton⁵⁴,
 A. Smetkina³⁸, E. Smith¹³, I.T. Smith⁵⁷, M. Smith⁶⁰, A. Snoch³¹, M. Soares¹⁹,
 L. Soares Lavra⁹, M.D. Sokoloff⁶⁴, F.J.P. Soler⁵⁸, B. Souza De Paula², B. Spaan¹⁴,
 E. Spadaro Norella^{25,p}, P. Spradlin⁵⁸, F. Stagni⁴⁷, M. Stahl⁶⁴, S. Stahl⁴⁷, P. Steffen⁴⁸,
 O. Steinkamp^{49,78}, S. Stemmler¹⁶, O. Stenyakin⁴³, M. Stepanova³⁷, H. Stevens¹⁴, S. Stone⁶⁷,
 S. Stracka²⁸, M.E. Stramaglia⁴⁸, M. Straticiu³⁶, S. Strokov⁸⁰, J. Sun²⁶, L. Sun⁷², Y. Sun⁶⁵,
 P. Svihra⁶¹, K. Swientek³⁴, A. Szabelski³⁵, T. Szumlak³⁴, M. Szymanski⁴⁷, S. Taneja⁶¹,
 Z. Tang³, T. Tekampe¹⁴, F. Teubert⁴⁷, E. Thomas⁴⁷, K.A. Thomson⁵⁹, M.J. Tilley⁶⁰,
 V. Tisserand⁹, S. T'Jampens⁸, M. Tobin⁶, S. Tolk⁴⁷, L. Tomassetti^{20,g}, D. Torres Machado¹,
 D.Y. Tou¹², E. Tournefier⁸, M. Traill⁵⁸, M.T. Tran⁴⁸, E. Trifonova⁷⁸, C. Trippl⁴⁸,
 A. Tsaregorodtsev¹⁰, G. Tuci^{28,o}, A. Tully⁴⁸, N. Tuning³¹, A. Ukleja³⁵, A. Usachov³¹,
 A. Ustyuzhanin^{41,79}, U. Uwer¹⁶, A. Vagner⁸⁰, V. Vagnoni¹⁹, A. Valassi⁴⁷, G. Valenti¹⁹,
 M. van Beuzekom³¹, H. Van Hecke⁶⁶, E. van Herwijnen⁴⁷, C.B. Van Hulse¹⁷, M. van Veghel⁷⁵,
 R. Vazquez Gomez⁴⁴, P. Vazquez Regueiro⁴⁵, C. Vázquez Sierra³¹, S. Vecchi²⁰, J.J. Velthuis⁵³,
 M. Veltri^{21,q}, A. Venkateswaran⁶⁷, M. Veronesi³¹, M. Vesterinen⁵⁵, J.V. Viana Barbosa⁴⁷,
 D. Vieira⁶⁴, M. Vieites Diaz⁴⁸, H. Viemann⁷⁴, X. Vilasis-Cardona^{44,l}, G. Vitali²⁸,
 A. Vitkovskiy³¹, A. Vollhardt⁴⁹, D. Vom Bruch¹², A. Vorobyev³⁷, V. Vorobyev^{42,w},
 N. Voropaev³⁷, R. Waldi⁷⁴, J. Walsh²⁸, J. Wang³, J. Wang⁷², J. Wang⁶, M. Wang³, Y. Wang⁷,
 Z. Wang⁴⁹, D.R. Ward⁵⁴, H.M. Wark⁵⁹, N.K. Watson⁵², D. Websdale⁶⁰, A. Weiden⁴⁹,
 C. Weisser⁶³, B.D.C. Westhenry⁵³, D.J. White⁶¹, M. Whitehead¹³, D. Wiedner¹⁴,
 G. Wilkinson⁶², M. Wilkinson⁶⁷, I. Williams⁵⁴, M. Williams⁶³, M.R.J. Williams⁶¹,
 T. Williams⁵², F.F. Wilson⁵⁶, W. Wislicki³⁵, M. Witek³³, L. Witola¹⁶, G. Wormser¹¹,
 S.A. Wotton⁵⁴, H. Wu⁶⁷, K. Wyllie⁴⁷, Z. Xiang⁵, D. Xiao⁷, Y. Xie⁷, H. Xing⁷¹, A. Xu⁴, J. Xu⁵,
 L. Xu³, M. Xu⁷, Q. Xu⁵, Z. Xu⁴, Z. Yang³, Z. Yang⁶⁵, Y. Yao⁶⁷, L.E. Yeomans⁵⁹, H. Yin⁷,

J. Yu⁷, X. Yuan⁶⁷, O. Yushchenko⁴³, K.A. Zarebski⁵², M. Zavertyaev^{15,c}, M. Zdybal³³,
M. Zeng³, D. Zhang⁷, L. Zhang³, S. Zhang⁴, W.C. Zhang^{3,y}, Y. Zhang⁴⁷, A. Zhelezov¹⁶,
Y. Zheng⁵, X. Zhou⁵, Y. Zhou⁵, X. Zhu³, V. Zhukov^{13,39}, J.B. Zonneveld⁵⁷, S. Zucchelli^{19,e}.

¹*Centro Brasileiro de Pesquisas Físicas (CBPF), Rio de Janeiro, Brazil*

²*Universidade Federal do Rio de Janeiro (UFRJ), Rio de Janeiro, Brazil*

³*Center for High Energy Physics, Tsinghua University, Beijing, China*

⁴*School of Physics State Key Laboratory of Nuclear Physics and Technology, Peking University, Beijing, China*

⁵*University of Chinese Academy of Sciences, Beijing, China*

⁶*Institute Of High Energy Physics (IHEP), Beijing, China*

⁷*Institute of Particle Physics, Central China Normal University, Wuhan, Hubei, China*

⁸*Univ. Grenoble Alpes, Univ. Savoie Mont Blanc, CNRS, IN2P3-LAPP, Annecy, France*

⁹*Université Clermont Auvergne, CNRS/IN2P3, LPC, Clermont-Ferrand, France*

¹⁰*Aix Marseille Univ, CNRS/IN2P3, CPPM, Marseille, France*

¹¹*Université Paris-Saclay, CNRS/IN2P3, IJCLab, Orsay, France*

¹²*LPNHE, Sorbonne Université, Paris Diderot Sorbonne Paris Cité, CNRS/IN2P3, Paris, France*

¹³*I. Physikalisches Institut, RWTH Aachen University, Aachen, Germany*

¹⁴*Fakultät Physik, Technische Universität Dortmund, Dortmund, Germany*

¹⁵*Max-Planck-Institut für Kernphysik (MPIK), Heidelberg, Germany*

¹⁶*Physikalisches Institut, Ruprecht-Karls-Universität Heidelberg, Heidelberg, Germany*

¹⁷*School of Physics, University College Dublin, Dublin, Ireland*

¹⁸*INFN Sezione di Bari, Bari, Italy*

¹⁹*INFN Sezione di Bologna, Bologna, Italy*

²⁰*INFN Sezione di Ferrara, Ferrara, Italy*

²¹*INFN Sezione di Firenze, Firenze, Italy*

²²*INFN Laboratori Nazionali di Frascati, Frascati, Italy*

²³*INFN Sezione di Genova, Genova, Italy*

²⁴*INFN Sezione di Milano-Bicocca, Milano, Italy*

²⁵*INFN Sezione di Milano, Milano, Italy*

²⁶*INFN Sezione di Cagliari, Monserrato, Italy*

²⁷*INFN Sezione di Padova, Padova, Italy*

²⁸*INFN Sezione di Pisa, Pisa, Italy*

²⁹*INFN Sezione di Roma Tor Vergata, Roma, Italy*

³⁰*INFN Sezione di Roma La Sapienza, Roma, Italy*

³¹*Nikhef National Institute for Subatomic Physics, Amsterdam, Netherlands*

³²*Nikhef National Institute for Subatomic Physics and VU University Amsterdam, Amsterdam, Netherlands*

³³*Henryk Niewodniczanski Institute of Nuclear Physics Polish Academy of Sciences, Kraków, Poland*

³⁴*AGH - University of Science and Technology, Faculty of Physics and Applied Computer Science, Kraków, Poland*

³⁵*National Center for Nuclear Research (NCBJ), Warsaw, Poland*

³⁶*Horia Hulubei National Institute of Physics and Nuclear Engineering, Bucharest-Magurele, Romania*

³⁷*Petersburg Nuclear Physics Institute NRC Kurchatov Institute (PNPI NRC KI), Gatchina, Russia*

³⁸*Institute of Theoretical and Experimental Physics NRC Kurchatov Institute (ITEP NRC KI), Moscow, Russia, Moscow, Russia*

³⁹*Institute of Nuclear Physics, Moscow State University (SINP MSU), Moscow, Russia*

⁴⁰*Institute for Nuclear Research of the Russian Academy of Sciences (INR RAS), Moscow, Russia*

⁴¹*Yandex School of Data Analysis, Moscow, Russia*

⁴²*Budker Institute of Nuclear Physics (SB RAS), Novosibirsk, Russia*

⁴³*Institute for High Energy Physics NRC Kurchatov Institute (IHEP NRC KI), Protvino, Russia, Protvino, Russia*

⁴⁴*ICCUB, Universitat de Barcelona, Barcelona, Spain*

⁴⁵*Instituto Galego de Física de Altas Enerxías (IGFAE), Universidade de Santiago de Compostela, Santiago de Compostela, Spain*

⁴⁶*Instituto de Física Corpuscular, Centro Mixto Universidad de Valencia - CSIC, Valencia, Spain*

- ⁴⁷ *European Organization for Nuclear Research (CERN), Geneva, Switzerland*
- ⁴⁸ *Institute of Physics, Ecole Polytechnique Fédérale de Lausanne (EPFL), Lausanne, Switzerland*
- ⁴⁹ *Physik-Institut, Universität Zürich, Zürich, Switzerland*
- ⁵⁰ *NSC Kharkiv Institute of Physics and Technology (NSC KIPT), Kharkiv, Ukraine*
- ⁵¹ *Institute for Nuclear Research of the National Academy of Sciences (KINR), Kyiv, Ukraine*
- ⁵² *University of Birmingham, Birmingham, United Kingdom*
- ⁵³ *H.H. Wills Physics Laboratory, University of Bristol, Bristol, United Kingdom*
- ⁵⁴ *Cavendish Laboratory, University of Cambridge, Cambridge, United Kingdom*
- ⁵⁵ *Department of Physics, University of Warwick, Coventry, United Kingdom*
- ⁵⁶ *STFC Rutherford Appleton Laboratory, Didcot, United Kingdom*
- ⁵⁷ *School of Physics and Astronomy, University of Edinburgh, Edinburgh, United Kingdom*
- ⁵⁸ *School of Physics and Astronomy, University of Glasgow, Glasgow, United Kingdom*
- ⁵⁹ *Oliver Lodge Laboratory, University of Liverpool, Liverpool, United Kingdom*
- ⁶⁰ *Imperial College London, London, United Kingdom*
- ⁶¹ *Department of Physics and Astronomy, University of Manchester, Manchester, United Kingdom*
- ⁶² *Department of Physics, University of Oxford, Oxford, United Kingdom*
- ⁶³ *Massachusetts Institute of Technology, Cambridge, MA, United States*
- ⁶⁴ *University of Cincinnati, Cincinnati, OH, United States*
- ⁶⁵ *University of Maryland, College Park, MD, United States*
- ⁶⁶ *Los Alamos National Laboratory (LANL), Los Alamos, United States*
- ⁶⁷ *Syracuse University, Syracuse, NY, United States*
- ⁶⁸ *Laboratory of Mathematical and Subatomic Physics , Constantine, Algeria, associated to ²*
- ⁶⁹ *School of Physics and Astronomy, Monash University, Melbourne, Australia, associated to ⁵⁵*
- ⁷⁰ *Pontifícia Universidade Católica do Rio de Janeiro (PUC-Rio), Rio de Janeiro, Brazil, associated to ²*
- ⁷¹ *Guangdong Provincial Key Laboratory of Nuclear Science, Institute of Quantum Matter, South China Normal University, Guangzhou, China, associated to ³*
- ⁷² *School of Physics and Technology, Wuhan University, Wuhan, China, associated to ³*
- ⁷³ *Departamento de Física , Universidad Nacional de Colombia, Bogota, Colombia, associated to ¹²*
- ⁷⁴ *Institut für Physik, Universität Rostock, Rostock, Germany, associated to ¹⁶*
- ⁷⁵ *Van Swinderen Institute, University of Groningen, Groningen, Netherlands, associated to ³¹*
- ⁷⁶ *Universiteit Maastricht, Maastricht, Netherlands, associated to ³¹*
- ⁷⁷ *National Research Centre Kurchatov Institute, Moscow, Russia, associated to ³⁸*
- ⁷⁸ *National University of Science and Technology “MISIS”, Moscow, Russia, associated to ³⁸*
- ⁷⁹ *National Research University Higher School of Economics, Moscow, Russia, associated to ⁴¹*
- ⁸⁰ *National Research Tomsk Polytechnic University, Tomsk, Russia, associated to ³⁸*
- ⁸¹ *University of Michigan, Ann Arbor, United States, associated to ⁶⁷*

^a *Universidade Federal do Triângulo Mineiro (UFMT), Uberaba-MG, Brazil*

^b *Laboratoire Leprince-Ringuet, Palaiseau, France*

^c *P.N. Lebedev Physical Institute, Russian Academy of Science (LPI RAS), Moscow, Russia*

^d *Università di Bari, Bari, Italy*

^e *Università di Bologna, Bologna, Italy*

^f *Università di Cagliari, Cagliari, Italy*

^g *Università di Ferrara, Ferrara, Italy*

^h *Università di Genova, Genova, Italy*

ⁱ *Università di Milano Bicocca, Milano, Italy*

^j *Università di Roma Tor Vergata, Roma, Italy*

^k *AGH - University of Science and Technology, Faculty of Computer Science, Electronics and Telecommunications, Kraków, Poland*

^l *DS4DS, La Salle, Universitat Ramon Llull, Barcelona, Spain*

^m *Hanoi University of Science, Hanoi, Vietnam*

ⁿ *Università di Padova, Padova, Italy*

^o *Università di Pisa, Pisa, Italy*

^p *Università degli Studi di Milano, Milano, Italy*

^q *Università di Urbino, Urbino, Italy*

^r *Università della Basilicata, Potenza, Italy*

^s *Scuola Normale Superiore, Pisa, Italy*

^t *Università di Modena e Reggio Emilia, Modena, Italy*

^u *Università di Siena, Siena, Italy*

^v *MSU - Iligan Institute of Technology (MSU-IIT), Iligan, Philippines*

^w *Novosibirsk State University, Novosibirsk, Russia*

^x *INFN Sezione di Trieste, Trieste, Italy*

^y *School of Physics and Information Technology, Shaanxi Normal University (SNNU), Xi'an, China*

^z *Universidad Nacional Autónoma de Honduras, Tegucigalpa, Honduras*